



# Multi-Physical Parameter Cross-Sectional Imaging of Quantitative Phase and Fluorescence by Integrated Multimodal Microscopy

Rajput, Sudheesh K. ; Matoba, Osamu ; Kumar, Manoj ; Quan, Xiangyu ; Awatsuji, Yasuhiro ; Tamada, Yosuke ; Tajahuerce, Enrique

---

**(Citation)**

IEEE Journal of Selected Topics in Quantum Electronics, 27(4):6801809

**(Issue Date)**

2021-07

**(Resource Type)**

journal article

**(Version)**

Version of Record

**(Rights)**

This work is licensed under a Creative Commons Attribution 4.0 License. For more information, see <https://creativecommons.org/licenses/by/4.0/>

**(URL)**

<https://hdl.handle.net/20.500.14094/90008313>



# Multi-Physical Parameter Cross-Sectional Imaging of Quantitative Phase and Fluorescence by Integrated Multimodal Microscopy

Sudheesh K Rajput, Osamu Matoba<sup>✉</sup>, *Member, IEEE*, Manoj Kumar<sup>✉</sup>, Xiangyu Quan<sup>✉</sup>, Yasuhiro Awatsuji<sup>✉</sup>, Yosuke Tamada<sup>✉</sup>, and Enrique Tajahuerce

**Abstract**—Integrated multimodal cross-sectional or volumetric imaging techniques give us fruitful information to understand the behavior or status of target objects such as biological samples. Most of the reported systems for this purpose are either time consuming due to scanning or use additional reference beams such as in interferometry. Therefore, fast, simple, highly efficient, and powerful multimodal imaging systems that can perform cross-sectional imaging with simple algorithms are worth to be investigated. In this paper, a multimodal technique for cross-sectional quantitative phase and fluorescence imaging with computational microscopy is presented. We combine cross-sectional fluorescence and quantitative phase imaging by using the transport of intensity equation (TIE) and numerical wave propagation. The amplitude and phase of the fluorescence light wave with partially spatial coherence are obtained from three defocused intensity patterns. The proposed hybrid imaging system is simple, compact, and non-iterative. We present experimental results of microbeads and fluorescent protein-labeled living cells of the moss *Physcomitrella patens* to demonstrate the performance of the proposed imaging system.

**Index Terms**—Fluorescence imaging, fresnel propagation, multimodal microscopy, phase imaging, transport of intensity equation.

## I. INTRODUCTION

**F**LUORESCENCE imaging enables the visualization of the functional details of samples by labeling certain molecules

Manuscript received October 8, 2020; revised February 5, 2021; accepted March 1, 2021. Date of publication March 11, 2021; date of current version March 30, 2021. This work was supported by Japan Society for the Promotion of Science (JSPS) KAKENHI (18H03888, 18H04790, 19H05274, 20H05886, 20H05887, 20H05891), JST CREST under Grant JPMJCR1755, and Frontier Photonic Sciences Project of National Institutes of Natural Sciences, 01212001. The work of Enrique Tajahuerce was supported by Generalitat Valenciana (PROMETEO/2020/029) and Ministerio de Ciencia e Innovación, MICINN (PID2019-110927RB-I00). (*Corresponding author: Osamu Matoba.*)

Sudheesh K Rajput, Osamu Matoba, Manoj Kumar, and Xiangyu Quan are with the Graduate School of System Informatics, Kobe University, Kobe, Hyogo 6578501, Japan (e-mail: srskrajput@gmail.com; matoba@kobe-u.ac.jp; manojklakra@gmail.com; zen@rabbit.kobe-u.ac.jp).

Yasuhiro Awatsuji is with the Faculty of Electrical Engineering and Electronics, Kyoto Institute of Technology, Kyoto 6068585, Japan (e-mail: awatsuji@kit.ac.jp).

Yosuke Tamada is with the School of Engineering, Utsunomiya University, Utsunomiya 3218585, Japan (e-mail: tamada@cc.utsunomiya-u.ac.jp).

Enrique Tajahuerce is with the Institute of New Imaging Technologies (INIT), Universitat Jaume I, Avda. Sos Baynat 12071, Castello, Spain (e-mail: enrique.tajahuerce@uji.es).

This article has supplementary material provided by the authors and color versions of one or more figures available at <https://doi.org/10.1109/JSTQE.2021.3064406>.

Digital Object Identifier 10.1109/JSTQE.2021.3064406

and structures. In fluorescence imaging for biological applications, an excitation light beam generally illuminates the sample through an objective lens that is also used to detect the emission from the sample [1]–[13]. A band pass filter separates the light by wavelength so that the emitted light can be imaged without interference from the excitation light [1]–[13]. Most of the fluorescence imaging techniques such as laser scanning confocal microscopy, two-photon microscopy, and other related techniques require a scanning process to get three-dimensional (3D) information [1]–[10]. These techniques are time-consuming for obtaining the 3D features of objects. Fast imaging techniques are highly desirable in the field of fluorescence imaging for measuring dynamic behavior of cellular activity and cellular network. For more large-scale observation in living animals, computational tomography of fluorescence and luminescence can be used [14]–[16].

On the other hand, phase imaging techniques have been used for obtaining structural information by exploiting optical path-length shifts through the specimen of interest [17]. Several techniques such as optical interferometry [18], single-pixel imaging and wavefront sensing [19], [20], ptychography [21] and transport of intensity equation imaging (TIE) [22]–[28], have been utilized for the visualization of phase information. Most of these techniques have been combined with fluorescence imaging to get additional functional information of the biological sample to be imaged [29]–[37].

When two or more physical parameters of a specimen are imaged together, the technique is usually named multimodal imaging [32]–[39]. Over the past decade, multi-modal imaging techniques that use phase imaging in combination with fluorescence imaging have been developed considerably due to several advantages [32]–[37]. In most of the multimodal imaging techniques, two or more setups are combined lowering the number of components, which can reduce the cost of the system up to some extent [32]–[39]. However, it enhances the complexity of the system. Besides, interferometric or scanning based configuration compromise the light efficiency or the temporal resolution of the imaging system, respectively. Therefore, imaging techniques that can perform two or more separate imaging modalities, by using a single optical setup to avoid complexity of the system, need to be investigated. Especially, investigations on multi-modal imaging systems to visualize and delineate the

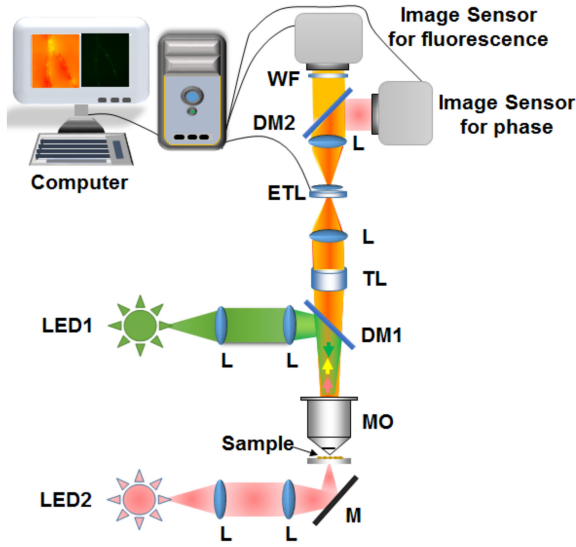


Fig. 1. Schematic of proposed 3D imaging setup. L: Lens, TL: Tube lens, ETL: Electrically tunable lens, MO: Microscope objective lens, M: Mirror, DM: Dichroic mirror, and WF: Wavelength filter. Here, LED1 is used to excite the sample for fluorescence imaging and LED2 is used to illuminate the sample for phase imaging. The use of suitable wavelength ranges of DM2 and WF separate the incoming light from sample for phase and fluorescence to be recorded by different image sensors. Image sensors and ETL are controlled by computer for recording the images for further processing.

structural and functional information in the biological specimen on a single platform at low light condition with simultaneous fast recording are in high demand. Furthermore, obtaining both features with simple and innovative 3D methods are at utmost demand for biological applications.

In this work, we propose a multimodal cross-sectional imaging of quantitative phase and fluorescence in an integrated system. Here, cross-sectional observation of both features are obtained by using the TIE algorithm and numerical refocusing using Fresnel propagation. The proposed system is simple and highly efficient due to non-involvement of any reference beam, in contrast with interferometric based multimodal imaging techniques. Our imaging technique also has the capability to obtain 3D features like holographic multimodal systems at lower cost (due to the use of inexpensive components) and with reduced light requirements (as it uses a single light beam technique). The performance of the proposed multimodal system is verified by conducting various experiments on fluorescent microspheres and fluorescent protein-labeled living cells of the moss *Physcomitrella patens* (*Physcomitrella*). In the case of fluorescence imaging, it is assumed that some degree of spatial coherence is available after the propagation with sufficient distance when the fluorescent objects are small enough and sparsely distributed.

## II. PROPOSED 3D IMAGING SYSTEM

The schematic diagram of the proposed imaging system, performing simultaneously quantitative phase and fluorescence imaging in arbitrary cross-sectional planes, is shown in Fig. 1. Two light sources and two image sensors are used. We note

that it is possible to use a single color image sensor to capture two light waves with different wavelengths. However, in the plant cell experiment, a high-sensitive image sensor is required to capture the weak fluorescence light to avoid optical damage of the plant cell. For fluorescence, a blue light-emitting diode (LED), denoted LED1 in Fig. 1, is used to excite the sample and another LED (LED2) is used for phase imaging. The light from LED1 is reflected from the dichroic mirror (DM1), which allows the light to enter the microscope objective lens (MO) to excite the fluorescent objects under study. The fluorescent light emitted by the objects passes through DM1 and then through the  $4f$  system after passing through a tube lens (TL). The  $4f$  imaging system also includes an electrically tunable lens (ETL) that is inserted in the focal plane between the two lenses. It should be noticed that the use of an ETL in this configuration allows us the recording of the stacks of images with slightly different focus without changing the magnification. A bandpass/wavelength filter (WF) is used to selectively record fluorescent light with the image sensor after passing through another dichroic mirror DM2. For phase imaging, LED2 is used to illuminate the sample. In this case, the light passes through the same components as in the case of fluorescence up to DM2, minimizing the requirement of components unlike other multimodal systems performing interferometric or holography based multimodal imaging. Finally, the reflected light from DM2 is recorded for phase imaging by another image sensor.

Firstly, we would like to discuss briefly the principle of TIE imaging and then how it can be used for 3D phase and fluorescence visualization. Basically, the TIE describes the relationship between the derivative of intensity with respect to the optical axis and the phase at the image plane. It can be written as follows [22]–[28]

$$-\frac{2\pi}{\lambda} \frac{\partial I_z(x, y)}{\partial z} = \nabla \cdot [I_z(x, y) \times \nabla \phi_z(x, y)], \quad (1)$$

where  $(x, y)$  are the spatial coordinates perpendicular to the optical axis,  $\lambda$  is the wavelength,  $I_z(x, y)$  is the in-focus intensity distribution, and  $\phi_z(x, y)$  is the phase distribution at the same plane. The symbol  $\nabla$  denotes the 2D gradient operator and  $z$  indicates the positions along the optical axis of the lateral plane  $(x, y)$ .

To solve the TIE for obtaining the phase distribution,  $\phi_0(x, y)$  [22]–[31], the following equation is used:

$$\phi_0(x, y) = -\frac{2\pi}{\lambda} FT^{-1} \text{Bigg} \left[ \frac{1}{4\pi^2(u^2 + v^2)} FT \left[ \nabla \cdot \frac{\nabla}{I_0(x, y)} \right] \times FT^{-1} \left\{ \frac{1}{4\pi^2(u^2 + v^2)} \times FT \left\{ \frac{\partial I_0(x, y)}{\partial z} \right\} \right\} \right] \quad (2)$$

Here,  $(u, v)$  represents the coordinates in the Fourier transform (FT) domain. Now, we assume that the object is located at a distance  $z$  along the optical axis. The intensity distribution,  $I_0(x, y)$  can be recorded by the optical setup as shown in Fig. 1 with the image sensor located at axial position  $z = 0$ , that is, at an out-of-focus plane. The intensity derivative used in (2) is

approximated using the difference of two additional intensity distributions,  $I_{\Delta z}(x, y)$  and  $I_{-\Delta z}(x, y)$ , obtained at different axial positions shifted  $\Delta z$  and  $-\Delta z$ . The relation between the derivative and the axially shifted intensity distributions can be written as-

$$\frac{\partial I_0(x, y)}{\partial z} = \frac{I_{\Delta z}(x, y) - I_{-\Delta z}(x, y)}{2\Delta z}, \quad (3)$$

Therefore, the retrieved phase distribution is obtained from (2) by using three intensity distributions shifted along the axial direction around  $z = 0$ . The complex amplitude distribution for the fluorescence and phase imaging,  $H(x, y)$ , is constructed by combining the phase distribution  $\phi_0(x, y)$ , obtained by TIE and the corresponding amplitude distribution  $I_0(x, y)$ . The retrieved complex amplitude distribution is Fresnel propagated to get the focused input image. The propagation distance gives us the depth information. The free space Fresnel propagation of the complex amplitude distribution,  $H(x, y)$ , is implemented by using the following equation:

$$C_z(\zeta, \eta) = \iint H(x, y) \exp \times \left[ \frac{i\pi}{\lambda z} \left( (\zeta - x)^2 + (\eta - y)^2 \right) \right] dx dy \quad (4)$$

The free space Fresnel propagation can be calculated numerically using a fast Fourier transform based algorithm [40].

The optical setup for simultaneous visualization of phase and fluorescence features is shown in Fig. 1. In both cases, three defocus intensity images are recorded and used to apply the TIE algorithm. The same procedure is followed to obtain the complex amplitude, as described through (1- 4), for the cases of fluorescence and phase modalities. For the case of phase imaging, the phase is retrieved by calculating the angle of the propagated complex distribution in (4), as follows-

$$\phi_z(\zeta, \eta) = \text{angle}[C_z(\zeta, \eta)] \quad (5)$$

It should be noted that the retrieved phase is wrapped continuously between 0 and  $2\pi$  and, therefore, a phase unwrapping process is required. The process of phase unwrapping involves the retrieval of the original (unwrapped) phase starting from the corresponding restricted (wrapped) phase in the  $(-\pi, \pi)$  or  $(0, 2\pi)$  interval. For the purpose of quantitative phase imaging, we remove the  $2\pi$  phase discontinuity by applying the Goldstein phase unwrapping algorithm [41, 42]. The phase distribution can be obtained at planes located at different axial distances  $z$  on the sample to get quantitative 3D phase information.

For the case of cross-sectional fluorescence imaging, the complex wave function obtained applying the TIE algorithm to the fluorescence intensity distribution is further Fresnel propagated to get intensity information at different depths. The retrieved intensity distribution,  $I_r(\xi, \eta)$  can be obtained as follows-

$$I_r(\zeta, \eta) = |C_z(\zeta, \eta)|^2 \quad (6)$$

Here, it is straightforward to reconstruct the different intensity images at planes located at different  $z$  distances to get cross-sectional distributions of the sample of interest.

It is well known that the light emitted from fluorescence objects is incoherent. However, in this study, our observation

target is constituted by fluorescent protein-labeled nucleus in living cells or fluorescence bead, which is assumed as a collection of quasi-point like fluorescent light sources due to its size of the order of  $10 \mu\text{m}$ . Further, a band-pass filter is used to increase the temporal coherence. Hence, we can consider that the light emitted by the fluorescence objects, after propagation through the optical system is partially coherent both spatially and temporally. Therefore, it is possible to measure the phase distribution associated to this partially coherent light proceeding from fluorescence of small objects [29], [31]. If the light source has points located at different distances, our technique based on TIE is able to detect the defocusing phase and, therefore, to reconstruct the light source at the original distance. This is also similar to other conventional 3D imaging techniques with incoherent light such as confocal imaging or integral imaging. In our system, the measured phase is related with the defocus transfer function, which will be different for fluorescent light sources located at different axial distances. By measuring the phase, we are measuring the transfer function of the optical system, and therefore we are able to focus to different distances.

### III. EXPERIMENTAL RESULTS

To perform the experiment for the demonstration of simultaneous cross-sectional fluorescence and quantitative phase imaging, the optical setup shown in Fig. 1 is used. A blue LED of 470 nm wavelength is used as excitation light source. The MO used in the experiment has a numerical aperture of 0.4 and a magnification of 20x, adapted for imaging living plant cells and microbeads of  $10.4 \mu\text{m}$  in diameter. The light emitted by the microbeads has a spectral bandwidth with wavelengths ranging from 450 nm to 600 nm. The strongest central wavelength emitted from the yellow fluorescent protein Citrine [43], [44] that labels nuclei in living cells is 529 nm. A band-pass/wavelength filter centered at 580 nm with a bandwidth of 10 nm is used to pass only fluorescence light in case of beads. On the other hand, for the imaging of fluorescent protein-labelled plant cells, a band pass filter of 525 nm with bandwidth of 39 nm is used.

For phase imaging, a LED with a wavelength of 560 nm is used as light source. And a band-pass/wavelength filter centered at  $550 \pm 10 \text{ nm}$  is used to block or reduce light from other sources. We have to note that part of fluorescence light, especially that arising from beads, also pass through the filter and reach the image sensor for phase imaging. However, the fluorescence light is much weaker than the transmitted light for phase imaging and does not affect the phase imaging technique. In the case of bead imaging, the size of the image sensor is  $1500 \times 1500$  pixels for fluorescence and phase, with a pixel pitch of  $6.5 \mu\text{m}$ , while in the case of plant-cell imaging, the size of the image sensor is  $700 \times 700$  pixels for fluorescence with a pixel pitch of  $3.45 \mu\text{m}$  and  $920 \times 920$  pixels for phase with a pixel pitch of  $4.54 \mu\text{m}$ . In both cases, three defocus intensity images are recorded by changing the optical power of the ETL (EL-16-40-TC by Optotune). The focal length of the lenses used for phase and fluorescence illumination is 100 mm. While the focal length of the lenses used in the 4f system is 150 mm.



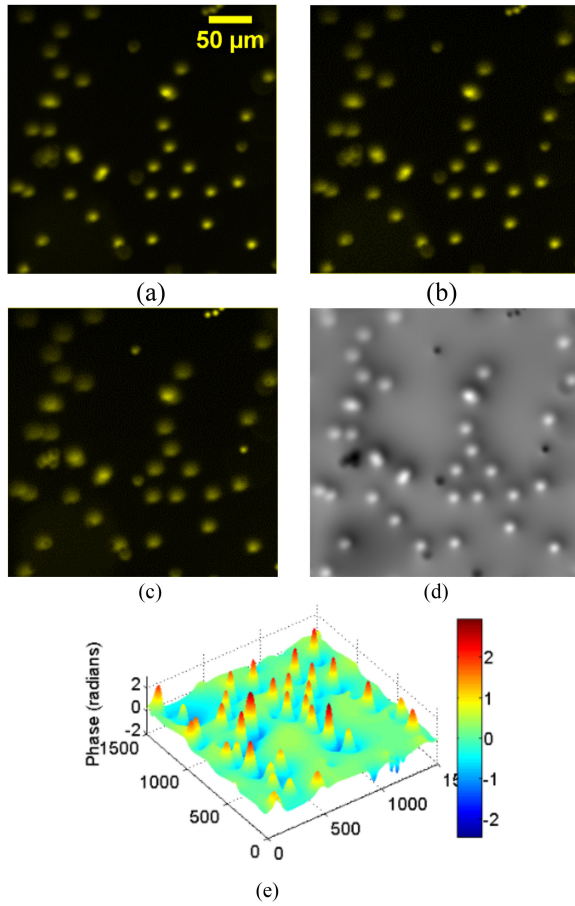


Fig. 2. Experimental results of cross-sectional fluorescence imaging. (a)–(c) Three defocused images of fluorescent microbeads, (d) the 2D phase distribution obtained from out of focus images in (a)–(c) by using the TIE algorithm. (e) quantitative phase profile. The fluorescence image shown in Fig. (b) and phase image shown in Fig. (d) are used for further processing to retrieve focused images.

The experimental results for simultaneous fluorescence and quantitative phase imaging of fluorescent microbeads are shown in Figs. 2 to 5. The results of simultaneous cross-sectional fluorescence imaging are shown in Figs. 2(a)–(e). The recording interval of axial distances of the defocused images to apply the TIE algorithm is  $3\ \mu\text{m}$ . Three defocus intensity images are recorded which are shown in Figs. 2(a)–(c). The extracted phase distribution obtained from these defocus images by the TIE algorithm is shown in Fig. 2(d) and the corresponding surface plot is shown in Fig. 2(e). The phase change (high phase value) can be noticed for all the beads falling under the field of view of the imaging system. This phase distribution and the corresponding intensity distribution constitute the complex distribution of propagated optical wave at a particular distance. Then, the intensity distributions at different distances are reconstructed numerically by propagating the complex amplitude distributions. Here, we present the reconstructed intensity images in two planes. The reconstruction distances are  $-33\ \text{mm}$  and  $32\ \text{mm}$  from the defocus image, which correspond to  $-82.5\ \mu\text{m}$  and  $80\ \mu\text{m}$  in the sample domain, respectively. The reconstruction results are shown in Figs. 3(a)–(f). The reconstructed

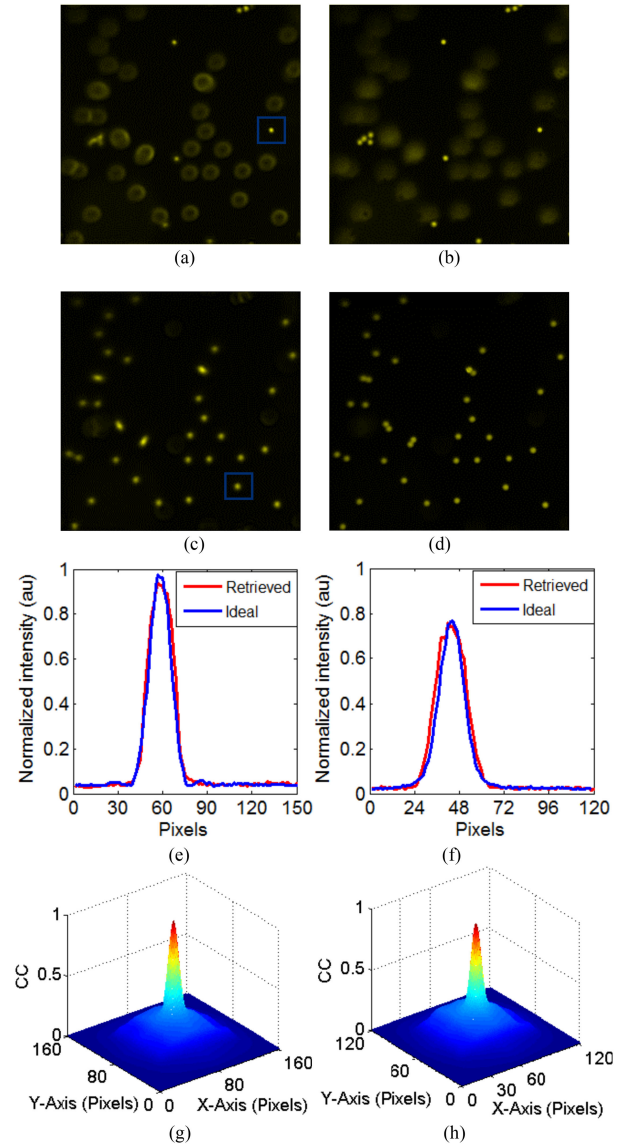


Fig. 3. Reconstruction results of cross-sectional fluorescence imaging. (a) recovered focused image when the first plane is in focus (in the selected region) after Fresnel propagation of complex function, (b) ideal focused image obtained by focusing the microscope experimentally to the first plane, (c) recovered focused image when the second plane is in focus (in the selected region) after Fresnel propagation of complex function, (d) ideal focused image obtained by focusing the microscope to the second plane, (e) comparison of intensity line profiles of images for the selected region in first plane focused computationally and optically, (f) comparison of intensity line profiles of images for the selected region in second plane obtained by focusing computationally and optically, (g) autocorrelation (the CC peak value is 1) of selected region in (a), and (h) the plot of the cross-correlation (the CC peak value is 0.93) between selected regions in (a) and (b). Here, the similarity between the line profiles confirms the ability of our system to obtain the focused images at different distances.

fluorescence image for the fluorescent beads of selected area in focus, is shown in Fig. 3(a). Fig. 3(c) is the reconstructed fluorescence image for the second plane, where another selected area is in focus. Fluorescence images are drastically changed by numerical refocusing. For comparison, in Figs. 3(b) and (d) we show the images recorded experimentally by focusing the microscope directly onto the same axial planes considered in

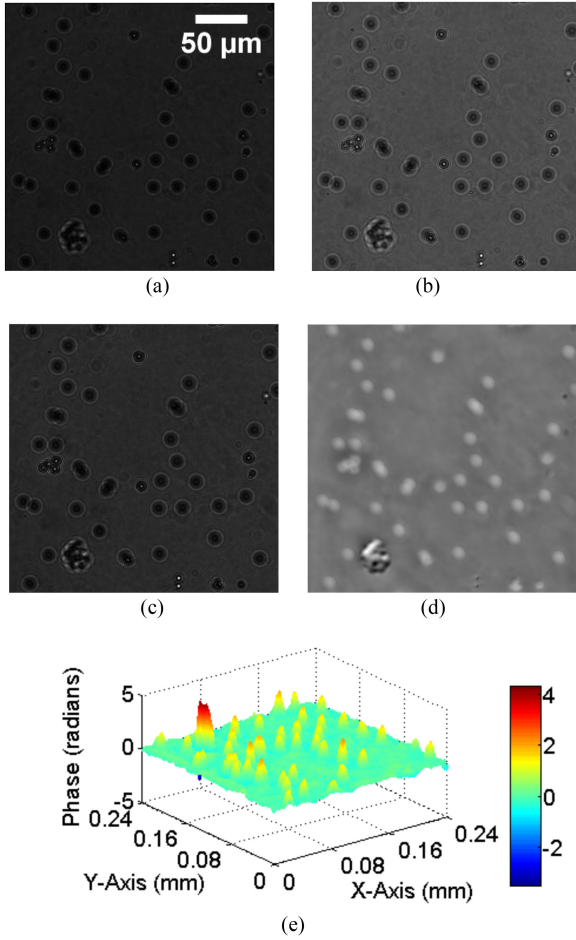


Fig. 4. Experimental results of multi-plane phase imaging. (a)–(c) Three out of focus images of microbeads, (d) the 2D phase distribution obtained from images (a)–(c) by using the TIE algorithm, and (e) quantitative phase profile. The intensity image shown in Fig. (b) and the phase image shown in Fig. (d) are used for further processing to retrieve other focused phase images.

Figs. 3(a) and (c), respectively. The normalized intensity profiles of images retrieved computationally and optically are shown in Fig. 3(e) for the first focused plane and in Fig. 3(f) for the second plane. Another comparison in terms of cross-correlation (CC) has also been carried out whose results are shown in Fig. 3(g) and (h). Firstly, we confirm that the autocorrelation of the selected region in Fig. 3(a) has a correlation peak value equal to 1, as it can be seen in the autocorrelation plot in Fig. 3(g). Second, we verify that the CC peak value is only slightly reduced to 0.93 when the correlation of the selected region is calculated between the image retrieved computationally, in Fig. 3(a), and that obtained optically, in Fig. 3(b). The correlation plot is shown in Fig. 3(h). From these results, it can be seen that fluorescence images at different distances can be reconstructed from defocus fluorescence images.

For phase imaging, the recorded three out of focus intensity images in transmission mode are shown in Figs. 4(a–c). The recording interval of axial distances for the out of focus images is 2  $\mu\text{m}$ . The output phase image obtained from these defocus images using the TIE algorithm is shown in Fig. 4(d) and the

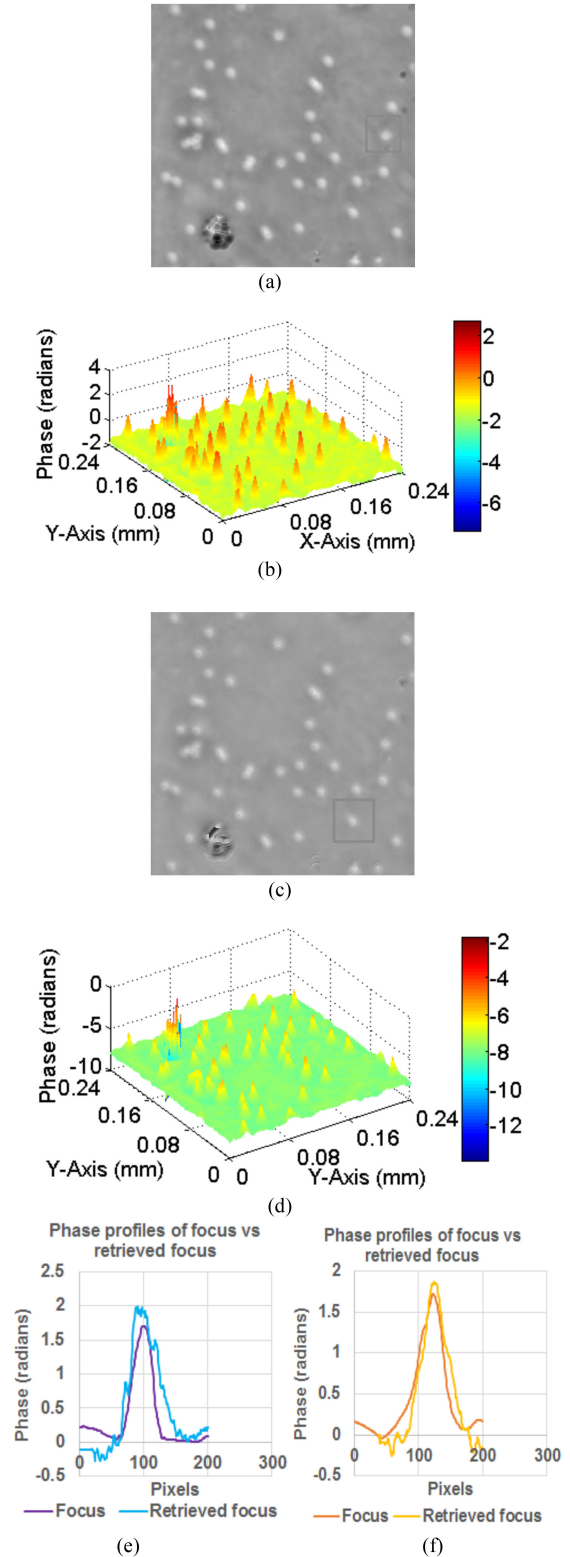


Fig. 5. Reconstruction results of multi-plane phase imaging. (a) 2D phase distribution at the first focused plane obtained after Fresnel propagation of the complex function, (b) quantitative phase profile when first plane is at focus, (c) 2D phase distribution of the second focused plane obtained after Fresnel propagation of complex function, (d) quantitative phase profile when second plane is at focus, (e) comparison of phase profiles of images focused optically vs computationally corresponding to selected area in Fig. 2(a), (f) comparison of phase profiles of images focused optically vs computationally corresponding to the selected area in Fig. 2(c).

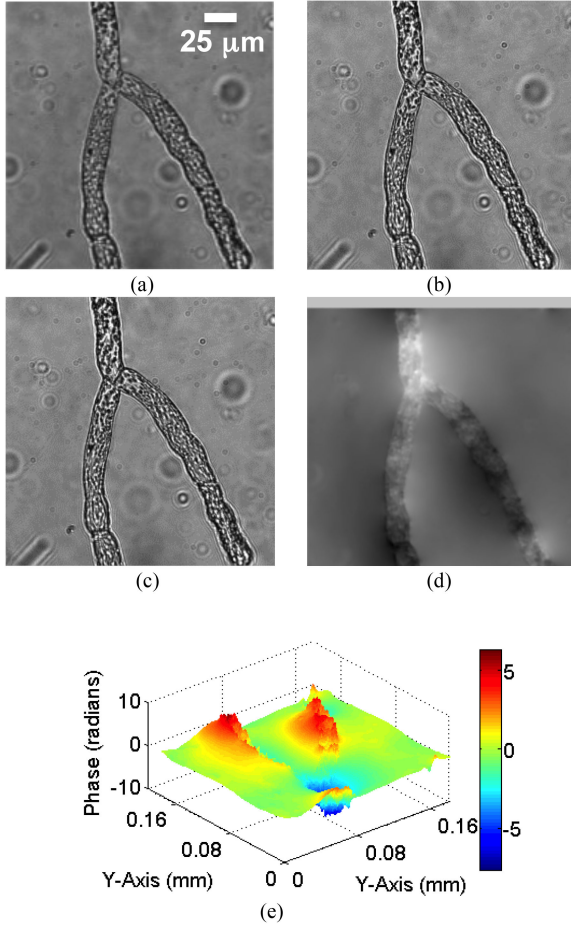


Fig. 6. Experimental results of multi-plane phase imaging of plant cells. (a)–(c) Three out of focus images of living plant cells, (d) 2D phase distribution reconstructed from defocused images by using the TIE algorithm, (e) 3D plot of the phase distribution.

corresponding quantitative phase distribution (surface plot) is shown in Fig. 4(e). The complex function obtained by multiplying the phase distribution in Fig. 4(d) with the defocus image in Fig. 4(b) is Fresnel propagated to reconstruct the desired phase distributions in different planes. We choose to reconstruct the phase in planes located at two different distances with different fluorescent beads in focus. The reconstruction distances are -12 mm and 55 mm from the defocus image, which correspond to  $-30\ \mu\text{m}$  and  $137.5\ \mu\text{m}$  in the sample domain, respectively. The reconstruction results are shown in Figs. 5(a–d). The reconstructed phase distribution for the first plane, where the fluorescent bead of the selected area is in focus, is shown in Fig. 5(a) and the corresponding phase distribution (surface plot) is shown in Fig. 5(b). Fig. 5(c) is the phase distribution for the second plane, where the fluorescent bead of the selected area is in focus, while the corresponding phase distribution (surface plot) is shown in Fig. 5(d). We have obtained also the phase distribution of these images focused optically in order to compare quantitatively the result obtained with both methods. The result of the comparison between profiles of the phase images obtained by computational and optical focusing are shown in Figs. 5(e) and (f). Fig. 5(e)

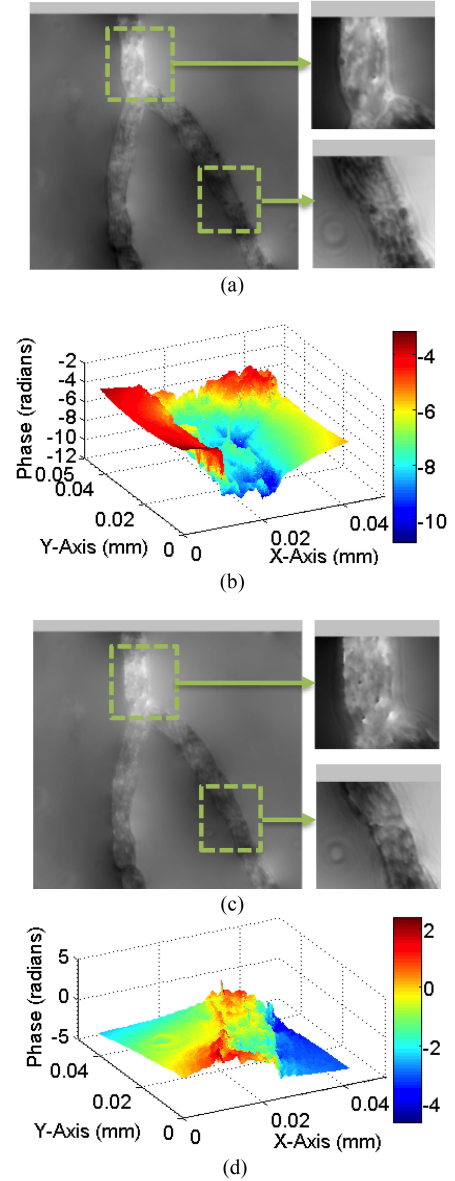


Fig. 7. Reconstruction results of multi-plane phase imaging of plant cells. (a) 2D phase distribution when upper plane is in focus, (b) 3D phase profile when upper plane is in focus (c) 2D phase distribution when lower plane is in focus, and (d) 3D plot of phase distribution when lower plane is in focus. Movie data (see Visualization 1) shows the cross-sectional reconstructed phase images.

shows the comparison of phase profiles corresponding to the selected area in Fig. 5(a) while Fig. 5(f) shows the comparison for the selected area in Fig. 5(c). From these results, it can be seen that quantitative phase images can be obtained at different axial distances starting from a defocused image obtained by TIE algorithms. Hence, the proposed system can successfully retrieve the multimodal 3D fluorescence and phase information simultaneously.

Another experiment is also carried out for the simultaneous quantitative phase and cross-sectional fluorescence imaging of living cells. *Physcomitrella* is chosen as an observation target [43], [45], where the Citrine Yellow fluorescent protein gene [44] was inserted into a histone H3.3 locus (Pp3c18\_14481)



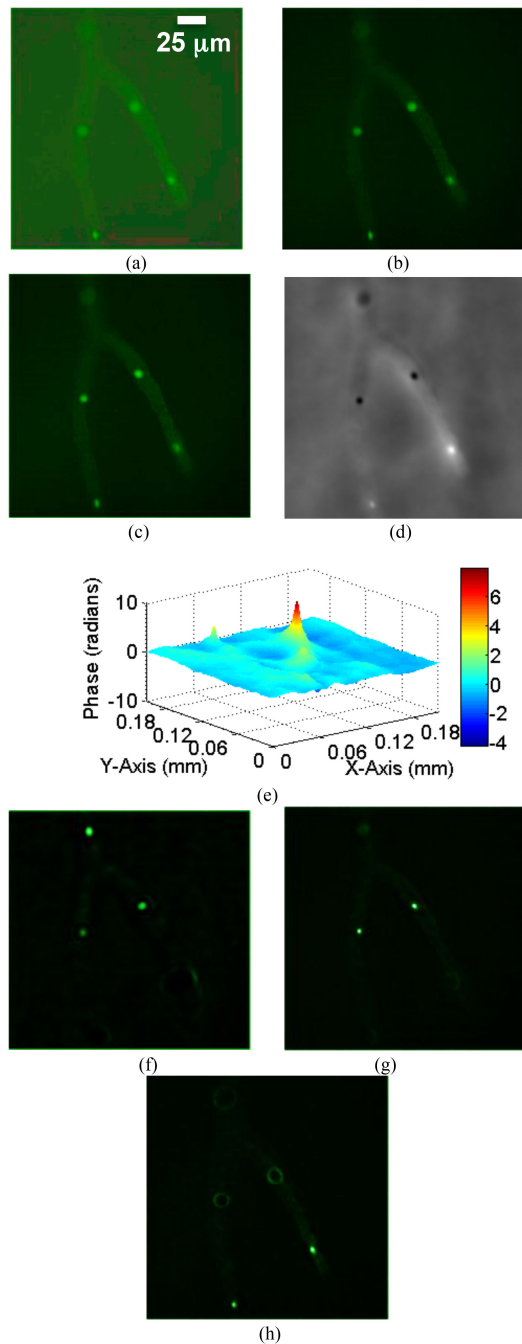


Fig. 8. Experimental results of 3D fluorescence imaging of plant cells. (a)–(c) Three defocused images of plant cells, (d) 2D phase distribution obtained from defocused images by using the TIE algorithm, (e) 3D plot of phase distribution, and the recovered focus images obtained after Fresnel propagation of complex function, (f) when upper plane is in focus, (g) when middle plane is in focus, and (h) when lower plane is in focus. The contrast of fluorescent images is enhanced by 30%. Movie data (see Visualization 2) shows the cross-sectional reconstructed fluorescence images.

to label only nuclei [46]. *Physcomitrella* has clear cell identity and relatively simple body structure [43], both of which are beneficial for molecular and developmental biological studies using imaging.

The results of plant-cell imaging are shown in Figs. 6 to 8. The results of cross-sectional quantitative phase imaging are shown

in Figs. 6 and 7 while cross-sectional fluorescence imaging results are shown in Fig. 8. Figs 6(a-c) show the three defocus images of the plant cells recorded with the image sensor for phase imaging in the multimodal microscope shown in Fig. 1. Fig. 6(d) shows the quantitative phase distribution obtained from the defocus images in Figs. 6(a-c) by applying the TIE algorithm. The 3D profile of the phase distribution is shown in Fig. 6(e). Fig. 7(a) shows the quantitative phase distribution in a first plane, located in the upper part of the sample, obtained after Fresnel propagation of the complex amplitude distribution. Fig. 7(b) shows the quantitative 3D profile of the phase distribution. The phase shifts are in the range of 5.5 radians and, therefore, we can estimate that the thickness of the cell is about 18.47  $\mu\text{m}$ , assuming that the refractive index of the plant cell is 1.36 [47], [48]. The obtained thickness is in the appropriate range of the actual thickness of the plant cell [43]. Fig. 7(c) shows the phase distribution in a second plane, located on the lower part of the sample, obtained after Fresnel propagation to the proper distance. Fig. 7(d) is the quantitative 3D phase profile of the lower area marked in Fig. 7(c). Movie data of reconstructed cross-sectional phase images is available (Visualization 1). The obtained reconstruction distances, for the first plane (upper part) and the second plane (lower part) are -3.6 mm and 2.9 mm, respectively, from the central out of focus image shown in Fig. 6(b).

Figs 8(a-c) are the three defocused images of plant cells recorded in fluorescence mode by the image sensor in Fig. 1. Fig. 8(d) shows the phase distribution obtained from the previous defocus images by the TIE algorithm. Fig. 8(e) shows the 3D profile of the quantitative phase distribution. Figs 8(f-h) show the recovered fluorescence images reconstructed at planes located at distances of -17 mm, -10 mm, and 6 mm, respectively, from the central defocused image. Movie data of reconstructed cross-sectional fluorescence images is available (Visualization 2). From these results obtained for plant cells, it can be claimed that the proposed multimodal imaging system is not only suitable for imaging standard objects but also for imaging biological samples in modern biology.

#### IV. CONCLUSION

In the presented work, we have proposed a non-interferometric multimodal computational imaging system for simultaneous quantitative phase and cross-sectional-fluorescence imaging that enables to visualize structural and functional features of biological samples. The proposed multimodal computational microscopy system is based on the TIE phase retrieval algorithm and Fresnel propagation. The 3D features of phase and fluorescence information are reconstructed by free space propagation from the complex amplitude distribution obtained previously with the help of the TIE algorithm. Both features of a sample in terms of fluorescence and phase images can be recorded and visualised simultaneously by using the same optical setup and by the same algorithm. The proposed imaging system is simple and shows a high efficiency, unlike holographic or interferometric imaging systems, and does not use iterative algorithms. We have presented experimental multimodal images



of microbeads and fluorescent protein-labeled living cells of *Physcomitrella*. From the presented results, it can be claimed that the proposed multimodal imaging system works successfully, providing simultaneous 3D fluorescence and phase images of a sample.

We hope that the strategies used in our proposed work will allow estimating phase from intensity to get cross-sectional/volumetric information in different experiments of advanced fluorescence imaging and other incoherent imaging methods.

**Conflicts of interest:** The authors declare no conflicts of interest.

## REFERENCES

- [1] B. N. Giepmans, S. R. Adams, M. H. Ellisman, and R. Y. Tsien, "The fluorescent toolbox for assessing protein location and function," *Science*, vol. 312, no. 5771, pp. 217–224, Apr. 2006.
- [2] J. W. Wang, A. M. Wong, L. B. V. J. Flores, and R. Axel, "Two-Photon calcium imaging reveals an odor-evoked map of activity in the fly brain," *Cell*, vol. 112, no. 2, pp. 271–282, Jan. 2003.
- [3] N. G. Horton *et al.*, "In vivo three-photon microscopy of subcortical structures within an intact mouse brain," *Nat. Photon.*, vol. 7, no. 3, pp. 205–209, Mar. 2013.
- [4] F. Helmchen and W. Denk, "Deep tissue two-photon microscopy," *Nat. Methods*, vol. 2, no. 12, pp. 932–940, Dec. 2005.
- [5] J. W. Lichtman and J. A. Conchello, "Fluorescence microscopy," *Nat. Methods*, vol. 2, no. 12, pp. 910–919, Dec. 2005.
- [6] J. Mertz, "Strategies for volumetric imaging with a fluorescence microscope," *Optica*, vol. 6, no. 10, pp. 1261–1268, Oct. 2019.
- [7] J. J. field, D. G. Winters, and R. A. Bartels, "Single-pixel fluorescent imaging with temporally labelled illumination patterns," *Optica*, vol. 3, no. 9, pp. 971–974, Sep. 2016.
- [8] G. Sancataldo, L. Silvestri, A. L. A. Mascaro, L. Sacconi, and F. S. Pavone, "Advanced fluorescence microscopy for in vivo imaging of neuronal activity," *Optica*, vol. 6, no. 6, pp. 758–765, Jun. 2019.
- [9] U. Kubitschek, *Fluorescence Microscopy: From Principles to Biological Applications*, 2nd ed., Hoboken, NJ, USA: Wiley-VCH, 2017.
- [10] K. S. Wells, D. R. Sandison, J. Strickler, and W. W. Webb, "Quantitative fluorescence imaging with laser scanning confocal microscopy," in *Handbook of Biological Confocal Microscopy*, Springer, Boston, MA, pp. 27–39, 1990.
- [11] S. You, C. Kuang, S. Li, X. Liu, and Z. Ding, "Three-dimensional super-resolution imaging for fluorescence emission difference microscopy," *AIP Adv.*, vol. 5, no. 8, Mar. 2015, Art. no. 084901.
- [12] Q. Ma *et al.*, "Three-dimensional fluorescent microscopy via simultaneous illumination and detection at multiple planes," *Sci. Rep.*, vol. 6, Art. no. 31445.
- [13] J. M. Jabbour *et al.*, "Optical axial scanning in confocal microscopy using an electrically tunable lens," *Biomed. Opt. Exp.*, vol. 5, no. 2, pp. 645–652, Feb. 2014.
- [14] M. Cai *et al.*, "Non-Negative iterative convex refinement approach for accurate and robust reconstruction in cerenkov luminescence tomography," *IEEE Trans. Med. Imag.*, vol. 39, no. 10, pp. 3207–3217, Oct. 2020.
- [15] M. Cai, Z. Zhang, X. Shi, Z. Hu, and J. Tian, "NIR-II/NIR-I fluorescence molecular tomography of heterogeneous mice based on gaussian weighted neighborhood fused lasso method," *IEEE Trans. Med. Imag.*, vol. 39, no. 6, pp. 2213–2222, Jun. 2020.
- [16] H. Guo *et al.*, "Weight multispectral reconstruction strategy for enhanced reconstruction accuracy and stability with cerenkov luminescence tomography," *IEEE Trans. Med. Imag.*, vol. 36, no. 6, pp. 1337–1346, Jun. 2017.
- [17] G. Popescu, *Quantitative Phase Imaging of Cells and Tissues*, New York, NY, USA: McGraw-Hill, 2011.
- [18] M. K. Kim, "Principles and techniques of digital holographic microscopy," *SPIE Rev.*, vol. 1, no. 1, May 2010, Art. no. 018005.
- [19] X. Hu *et al.*, "Single-pixel phase imaging by fourier spectrum sampling," *Appl. Phys. Lett.*, vol. 114, no. 5, Feb. 2019, Art. no. 051102.
- [20] F. Soldevila, V. Durán, P. Clemente, J. Lancis, and E. Tajahuerce, "Phase imaging by spatial wavefront sampling," *Optica*, vol. 5, no. 2, pp. 165–175, Feb. 2018.
- [21] X. Ou, R. Horstmeyer, C. Yang, and G. Zheng, "Quantitative phase imaging via fourier ptychographic microscopy," *Opt. Lett.*, vol. 38, no. 22, pp. 4845–4848, Nov. 2013.
- [22] D. Paganin and K. A. Nugent, "Non interferometric phase imaging with partially coherent light," *Phys. Rev. Lett.*, vol. 80, no. 12, pp. 2586–2589, Mar. 1998.
- [23] C. Zuo, Q. Chen, W. Qu, and A. Asundi, "High-speed transport-of-intensity phase microscopy with an electrically tunable lens," *Opt. Exp.*, vol. 21, no. 20, pp. 24060–24075, Oct. 2013.
- [24] W. Yu *et al.*, "Real time quantitative phase microscopy based on single-shot transport of intensity equation (ssTIE) method," *Appl. Phys. Lett.*, vol. 109, no. 7, Aug. 2016, Art. no. 071112.
- [25] X. Tian *et al.*, "Real-time quantitative phase imaging based on transport of intensity equation with dual simultaneously recorded field of view," *Opt. Lett.*, vol. 41, no. 7, pp. 1427–1430, Apr. 2016.
- [26] C. H. Chen, H. F. Hsu, H. R. Chen, and W. F. Hsieh, "Non-interferometric phase retrieval using refractive index manipulation," *Sci. Rep.*, vol. 7, Art. no. 46223.
- [27] X. Tian *et al.*, "In-focus quantitative intensity and phase imaging with the numerical focusing transport of intensity equation method," *J. Opt.*, vol. 18, no. 10, Oct. 2016, Art. no. 105302.
- [28] K. Komuro and T. Nomura, "Object plane detection and phase amplitude imaging based on transport of intensity equation," *Opt. Rev.*, vol. 24, no. 5, pp. 626–633, Oct. 2017.
- [29] S. K. Rajput *et al.*, "Three-dimensional fluorescence imaging using the transport of intensity equation," *J. Biomed. Opt.*, vol. 25, no. 3, Feb. 2019, Art. no. 032004.
- [30] J. Rosen and G. Brooker, "Non-scanning motionless fluorescence three-dimensional holographic microscopy," *Nat. Photon.*, vol. 2, pp. 190–195, Feb. 2008.
- [31] X. Quan *et al.*, "Three-dimensional stimulation and imaging-based functional optical microscopy of biological cells," *Opt. Lett.*, vol. 43, no. 21, pp. 5447–5450, Nov. 2018.
- [32] Y. Liu, J. Suo, Y. Zhang, and Q. Dai, "Single-pixel phase and fluorescence microscope," *Opt. Exp.*, vol. 26, no. 25, pp. 32451–32462, Dec. 2018.
- [33] R. P. Baker, M. J. Taormina, M. Jemielita, and R. Parthasarathy, "A combined light sheet fluorescence and differential interference contrast microscope for live imaging of multicellular specimens," *J. Microsc.*, vol. 258, no. 2, pp. 105–112, Dec. 2015.
- [34] Y. Park, G. Popescu, K. Badizadegan, R. R. Dasari, and M. S. Feld, "Diffraction phase and fluorescence microscopy," *Opt. Exp.*, vol. 14, no. 18, pp. 8263–8268, Sep. 2006.
- [35] X. Quan, K. Nitta, O. Matoba, P. Xia, and Y. Awatsuji, "Phase and fluorescence imaging by combination of digital holographic microscopy and fluorescence microscopy," *Opt. Rev.*, vol. 22, pp. 349–353, Apr. 2015.
- [36] X. Quan, O. Matoba, P. Xia, and Y. Awatsuji, "Image recovery from defocused 2D fluorescent images in multimodal digital holographic microscopy," *Opt. Lett.*, vol. 42, no. 9, pp. 1796–1799, May 2017.
- [37] J. Zheng, C. Zuo, P. Gao, and G. U. Nienhaus, "Dual-mode phase and fluorescence imaging with a confocal laser scanning microscope," *Opt. Lett.*, vol. 43, no. 22, pp. 5689–5692, Nov. 2018.
- [38] O. Matoba, X. Quan, P. Xia, Y. Awatsuji, and T. Nomura, "Multimodal imaging based on digital holography," *Proc. IEEE*, vol. 105, no. 5, pp. 906–923, May 2017.
- [39] T. Tahara, X. Quan, R. Otani, Y. Takaki, and O. Matoba, "Digital holography and its multidimensional imaging applications: A review," *Microscopy*, vol. 67, no. 2, pp. 55–67, Feb. 2018.
- [40] D. P. Kelly, "Numerical calculation of the fresnel transform," *J. Opt. Soc. Am. A*, vol. 31, no. 4, pp. 755–764, Apr. 2014.
- [41] L. L. García, A. G. Arellano, and W. C. Santos, "A parallel path-following phase unwrapping algorithm based on a top-down breadth-first search approach," *Opt. Lasers Eng.*, vol. 124, Jan. 2020, Art. no. 105827.
- [42] R. M. Goldstein, H. A. Zebker, and C. L. Werner, "Satellite radar interferometry: Two-dimensional phase unwrapping," *Rad. Sci.*, vol. 23, no. 4, pp. 713–720, Jul. 1988.
- [43] R. Kofuji and M. Hasebe, "Eight types of stem cells in the life cycle of the moss *Physcomitrella patens*," *Curr. Opin. Plant Biol.*, vol. 17, pp. 13–21, Feb. 2014.
- [44] A. A. Heikal, S. T. Hess, G. S. Baird, R. Y. Tsien, and W. W. Webb, "Molecular spectroscopy and dynamics of intrinsically fluorescent proteins: Coral red (dsRed) and yellow (Citrine)," *Proc. Natl. Acad. Sci. USA*, vol. 97, no. 22, pp. 11996–12001, Oct. 2000.
- [45] D. Lang *et al.*, "The *physcomitrella patens* chromosome - scale assembly reveals moss genome structure and evolution," *Plant J.*, vol. 93, pp. 515–533, Dec. 2018.

- [46] M. Kumar *et al.*, "Common-path multimodal three-dimensional fluorescence and phase imaging system," *J. Biomed. Opt.*, vol. 25, no. 3, Feb. 2020, Art. no. 032010.
- [47] X. J. Liang, A. Q. Liu, C. S. Lim, T. C. Ayi, and P. H. Yap, "Determining refractive index of single living cell using an integrated microchip," *Sens. Actuator A-Phys.*, vol. 133, pp. 349–354, Jul. 2007.
- [48] W. Choi *et al.*, "Tomographic phase microscopy," *Nat. Methods*, vol. 4, no. 9, pp. 717, Sep. 2007.



**Sudheesh K Rajput** received the B.S. and M.S. degrees in physics from Chhatrapati Shahu Ji Maharaj University, Kanpur, India, in 2006 and 2008, respectively, and the Ph.D. degree in optics from the Indian Institute of Technology Patna, Dayalpur Daulatpur, India, in 2015. He is an Assistant Professor with Kobe University, Kobe, Japan. His research interests include optical security, optical sound-field imaging, digital holography, and transport of intensity equation imaging and multimodal systems for fluorescence and phase imaging.



**Osamu Matoba** (Member, IEEE) received the Ph.D. degree in applied physics from Osaka University, Osaka, Japan, in 1996.

From 1996 to 2002, he was a Research Associate with the Institute of Industrial Science, University of Tokyo. From 2002 to 2009, he was an Associate Professor with the Department of Computer Science and Systems Engineering, Kobe University, Kobe, Japan. He is currently a Professor with the Department of Systems Science, Graduate School of System Informatics, Kobe University. His research interests

include optical sensing including digital holography, holographic 3D display, OCT, holographic memory, and artificial control of scattering phenomena.

Dr. Matoba is a Fellow of SPIE and OSA, and a Member of the Optical Society of Japan, and the Japan Society of Applied and a Member of IEEE and the Optical Society IEEE Donald G. Fink prized paper award in 2008.



**Manoj Kumar** received the M.Tech. degree in instrumentation from the National Institute of Technology, Kurukshetra, India, in 2011 and the Ph.D. degree in optical engineering from the Indian Institute of Technology Delhi, New Delhi, India, in 2016. From 2016 to 2017, he was a Postdoctoral Research Fellow with the Ben Gurion University of the Negev, Beer-sheba, Israel, from 2017 to 2019, JSPS Postdoctoral Research Fellow with Kobe University, Kobe, Japan, and currently a Project Assistant Professor with the Graduate School of System Informatics, Kobe University.

His research interests include 3D imaging, digital holography, 3D fluorescence microscopy, quantitative phase imaging, biomedical optics, and speckle metrology. He is a Member of the Optical Society of America.



**Xiangyu Quan** received the B.S. degree from the Beijing Information Science & Technology University, Beijing, China, and the M.E. and D.E. degrees from Kobe University, Kobe, Japan, in 2015 and 2017, respectively. He is currently an Assistant Professor with the Department of System Informatics, Kobe University. Her research interests include quantitative phase imaging microscopy, 3D fluorescence microscopy and optogenetic light stimulations tools by digital holographic methods. She is a Member of OSA and SPIE.



**Yasuhiro Awatsuji** received the B.E., M.E., and D.E. degrees in applied physics from Osaka University, Osaka, Japan, in 1992, 1994, and 1997, respectively.

From 1997 to 2005, he was a Research Associate with the Division of Information and Production Science, Kyoto Institute of Technology, Kyoto, Japan, where from 2005 to 2014, he was an Associate Professor with the Division of Electronics, and since 2014, has been a Professor with the Division of Electronics, Graduate School of Science and Technology. From 2005 to 2009, he was a Researcher with Precursory

Research for Embryonic Science and Technology, Japan Science and Technology Agency. His research interests include information optics with emphasis on holography, 3D display, 3D measurement, ultrafast optics, optics design, and optical information processing.

Dr. Awatsuji is a Senior Member of the Optical Society and the International Society for Optics and Photonics, and a Member of the Japan Society of Applied Physics and the Optical Society of Japan.



**Yosuke Tamada** received the bachelor's degree in agriculture, and the master's and Ph.D. degrees in life science from Kyoto University, Kyoto, Japan, in 2000, 2002, and 2005, respectively. He was a Postdoctoral Researcher with the University of Wisconsin-Madison until 2009 and an Assistant Professor with the National Institute for Basic Biology in Japan until 2019. He is currently an Associate Professor with Utsunomiya University, Utsunomiya, Japan. His current research interests include live-cell imaging, optical cell manipulation, and developmental biology

using plants. He is a Member of the Optical Society of Japan.



**Enrique Tajahuerce** received the Ph.D. degree in physics from Universidad de Valencia, Valencia, Spain, in 1998. He is currently an Associate Professor with the Department of Physics, Universitat Jaume I, Castelló, Spain, where he belongs to the Institute of New Imaging Technologies. From 1989 to 1992, he was a Research Technician with the Institute of Optics, Valencia. From 1999 to 2000, he was Postdoctoral Researcher with the University of Connecticut, Mansfield, CT, USA. His research interests include diffractive optics, adaptive optics, digital holography,

computational imaging, and imaging through scattering. He is a Fellow of OSA and Senior Member of SPIE. He was the recipient of the IEEE Donald G. Fink prized paper award in 2008.